CORE
Metadata, citation and similar papers at core.ac.uk
Provided by University of Dayton

University of Dayton
eCommons

Electro-Optics and Photonics Faculty Publications | Department of Electro-Optics and Photonics

6-2004

Interferometric and Holographic Imaging of Surface-Breaking Cracks

James Lawrence Blackshire
University of Dayton

Bradley D. Duncan
University of Dayton, bduncan1@udayton.edu

Follow this and additional works at: https://ecommons.udayton.edu/eop_fac_pub


Part of the Electromagnetics and Photonics Commons, Optics Commons, and the Other Physics Commons

eCommons Citation

Blackshire, James Lawrence and Duncan, Bradley D., "Interferometric and Holographic Imaging of Surface-Breaking Cracks" (2004). *Electro-Optics and Photonics Faculty Publications*. 23.
https://ecommons.udayton.edu/eop_fac_pub/23

This Article is brought to you for free and open access by the Department of Electro-Optics and Photonics at eCommons. It has been accepted for inclusion in Electro-Optics and Photonics Faculty Publications by an authorized administrator of eCommons. For more information, please contact frice1@udayton.edu, mschlangen1@udayton.edu.

Interferometric and holographic imaging of surface-breaking cracks

James L. Blackshire, MEMBER SPIE
Air Force Research Laboratory
Wright-Patterson Air Force Base
Ohio 45433
and
University of Dayton
Electro-Optics Graduate Program
Dayton, Ohio 45469

Bradley D. Duncan, MEMBER SPIE
University of Dayton
Electro-Optics Graduate Program
Dayton, Ohio 45469

Abstract. Two advanced nondestructive evaluation systems are developed for imaging surface-breaking cracks in aerospace materials. The systems use scanning heterodyne interferometry and frequency-translated holography principles to image ultrasonic displacement fields on material surfaces with high resolution and sensitivity. Surface-breaking cracks are detected and characterized by visualizing near-field ultrasonic scattering processes, which in turn results in local intensification of ultrasonic displacement fields in the immediate vicinity of a crack. The local intensification permits cracks to be easily distinguished from background levels, and creates unique displacement field images that follow the contours and morphology of the cracks with microscopic precision. The interferometric and holographic imaging approaches each provide noncontact and near optical-diffraction-limited measurement capabilities that are essential for probing ultrasonic displacement fields in the immediate vicinity of cracks. Several representative crack-imaging results are provided, along with detailed descriptions of both experimental techniques, and the capabilities and limitations of each method. The resulting systems provide simple yet very powerful tools for evaluating surface-breaking cracks in detail. © *2004 Society of Photo-Optical Instrumentation Engineers.* [DOI: 10.1117/1.1731201]

Subject terms: heterodyne interferometry; real-time holography; nondestructive evaluation.

Paper 030369 received Jul. 29, 2003; revised manuscript received Dec. 15, 2003; accepted for publication Dec. 31, 2003.

1 Introduction

For more than 60 years, simple detection and basic sizing of cracks has been the primary goal of nondestructive evaluation (NDE) crack measurements.[1,2] A wide variety of NDE techniques have been applied to the crack detection/characterization problem, with current state of the art systems providing detection capabilities approaching 100 μm in length and 10 μm in depth.[3–5] However, the vast majority of these systems provide only limited information regarding crack location and basic size.[1,6–8]

A recent trend in NDE research involves the development of advanced systems capable of characterizing surface-breaking cracks in full 2- or 3-D detail. Some of the most notable systems include laser ultrasonic,[9,10] photoinductive,[11] and sonic infrared imaging.[12] In addition to providing basic detection and sizing measurements, each of these advanced techniques provide a capability for *visualizing* a crack and its local surroundings. As research tools, they provide unprecedented access to crack initiation and growth processes and, for example, allow the detailed study of crack-tip/microstructure interactions, crack branching, multicrack systems, and stress-corrosion crack growth processes. As an engineering assessment tool, the complete characterization of a detected crack will significantly enhance the reliability of structural integrity and life-prediction assessments.

In this effort, two advanced laser ultrasonic NDE systems were developed for the expressed purpose of imaging surface-breaking cracks in aerospace alloys. The techniques use interferometric and holographic approaches to visualize ultrasonic displacement fields propagating along the surface of a material. Surface-breaking cracks are detected and characterized through their ultrasonic scattering signatures, which in the ultrasonic near field of the crack site is dominated by free-boundary reflection processes. Free-boundary reflection processes create enhanced displacement levels that are highly localized near the defect site, and are easily separated from background levels. The interferometric and holographic systems probe these near-field regions with microscopic spatial resolution levels, providing a visualization of local crack-scattering processes, and thus an advanced NDE imaging capability for detecting and characterizing surface-breaking cracks.

2 Technical Background

Optical interferometry and holography techniques provide effective means for measuring surface motions and vibrations on nanometer scales, and have been used extensively in a number of different applications.[13–16] For ultrasonic NDE measurements, light scattered from each point on a vibrating object is phase modulated with a modulation depth proportional to the vibrational amplitude occurring at each point. By interfering this phase-modulated object light with an appropriate reference, the local vibration amplitude

 0091-3286/2004/$15.00 © 2004 Society of Photo-Optical Instrumentation Engineers

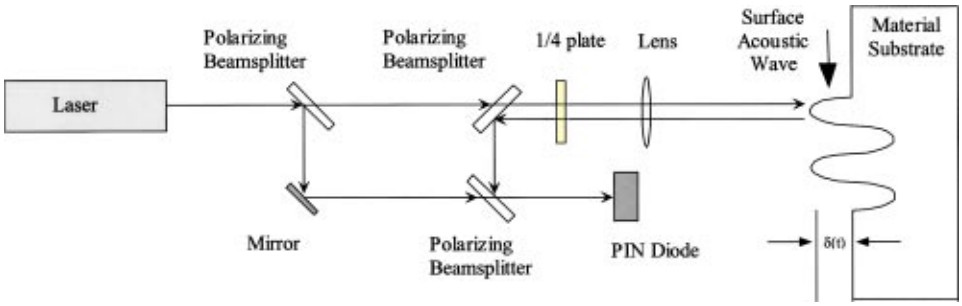

Fig. 1 Schematic diagram of a modified Mach-Zehnder interferometer system used to monitor surface displacements at a single point.

can be represented as an optical intensity that can be used to image the ultrasonic displacement field on a material surface.

2.1 *Interferometric Imaging of Ultrasound Fields*

There are two basic approaches for acquiring displacement-field images. The first approach involves the use of a focused laser beam to probe the material surface at a single point. This situation is depicted in Fig. 1 for a modified Mach-Zehnder interferometric setup. Recall that when a laser beam is reflected from a vibrating surface, with normal surface displacement $\delta(t)$, the corresponding optical path length change is twice the surface displacement, namely $2\delta(t)$. This introduces a phase change in the reflected laser beam of $2k\delta(t)$, where k is the wavenumber of the laser light. The interferometric recording process then combines the phase-shifted probe beam with a reference light source, resulting in a total field amplitude at the detector that is simply the additive combination of the individual components. The detected intensity can then be calculated from the total field amplitude multiplied by its complex conjugate, yielding

$$I = 1/2A^2[1+\cos(\Delta\phi)] = A^2\cos^2(\Delta\phi/2), \quad (1)$$

where reference and probe beams of equal amplitude A have been assumed, and where the differential phase term $\Delta\phi$ depends on the nominal phase difference ϕ_0 between the reference and probe beams, and the time-dependent material surface displacement $2\delta(t)$; that is,

$$\Delta\phi = \phi_0 + 2k\delta(t). \quad (2)$$

The interferometric signal described by Eqs. (1) and (2) is linear with respect to $\delta(t)$ if the following two conditions are met: 1. $\phi_0 = (2N-1)\pi/2$, where N is an integer; and 2. $\delta(t) \ll \lambda$. The nominal phase difference ϕ_0 can easily be adjusted to meet the first condition, and in practice the surface displacements are indeed much smaller than the optical wavelength. For example, if Nd:YAG light is used, the optical wavelength of $\lambda = 532$ nm is approximately one hundred times larger than a typical surface acoustic wave (SAW) amplitude of $h = 5$ nm, as we show in the results in Sec. 5. The interferometric signal, therefore, provides a detailed and precise measurement of the time-dependent motions of a vibrating material surface at a single point. For repetitive, acoustically driven surface displacements, the interferometry system can be synchronized to the motion source (e.g., a piezoelectric transducer attached to the material). By then raster scanning the interferometric probe beam position relative to the material surface, and taking into account the necessary synchronization requirements, a complete 2-D displacement-field image can be generated of the vibrating material surface.

2.2 *Holographic Imaging of Ultrasound Fields*

Frequency-translated holography provides an additional capability for visualizing surface displacement patterns as full-field images.[17–19] A schematic diagram of a typical experimental setup is depicted in Fig. 2. The system is based on a temporally modulated holography concept originally reported by Aleskoff,[17] and later developed into a SAW visualization system by Shiokawa, Moriizumi, and Yasuda.[19] As described by Aleskoff,[17] the hologram acts as a narrow bandpass filter, and records a stationary interference pattern in the holographic film if the object and reference beams are precisely matched in optical frequency. The SAW, acting like a traveling phase-grating structure, diffracts and frequency shifts the object beam into separate orders. As we show later, information about the local displacement amplitude of the SAW is contained predominantly in the ± 1 diffracted orders. These orders can be selected independently by using an appropriate spatial filter, as shown in Fig. 2. A full-field holographic visualization of the SAW amplitude distribution results when the reference beam is frequency shifted by an amount identical

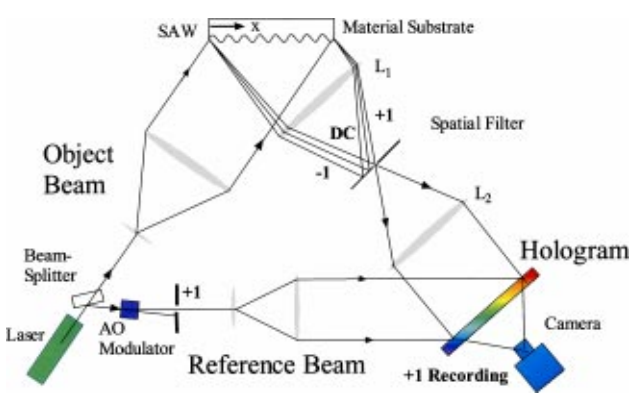

Fig. 2 Schematic diagram of a frequency-translated holography system capable of making 2-D, displacement-field images of a vibrating surface.

to the object beam. This can be accomplished, for example, by placing an acousto-optic (AO) modulator in the reference beam path.

Mathematically, the SAW can be described by the function $u_{saw}=h\sin(\Omega t-Kx)$, where h is the amplitude, Ω is the angular frequency, x is the position along the direction of propagation, $K=2\pi/\Lambda$ is the SAW wavenumber, and Λ is the SAW wavelength. For collimated light of wavelength λ, incident at an angle θ with respect to the surface normal of the material, the scattered optical field can be written in phasor form as

$$E_{obj}=E_0\exp\left[i\frac{2\pi}{\lambda}(2h\cos\theta)\sin(\Omega t-Kx)\right], \tag{3}$$

where ω is the angular frequency of the light wave and E_0 is its amplitude. As described by Duncan,[16] Eq. (3) can be simplified significantly by introducing a phase modulation index term $\beta=(4\pi h/\lambda)\cos\theta$, and by using the Bessel function identity

$$\exp[i\beta\sin(\Phi)]=\sum_{n=-\infty}^{n=\infty}J_n(\beta)\exp(in\Phi), \tag{4}$$

where J_n is Bessel's function of the first kind, order n. In practice, the SAW amplitude h is small compared to the optical wavelength λ, which means the phase modulation index β is also small. This allows the summation in Eq. (4) to be represented by only the 0, $+1$, and -1 terms. Then, if we recall that for small β, $J_0(\beta)\sim 1$, while $J_{+1}(\beta)\sim+\beta/2$, and $J_{-1}(\beta)\sim-\beta/2$,[20] Eq. (3) can be rewritten in the relatively simple form

$$E_{obj}\propto 1+\beta/2\exp[i(\Omega t-Kx)]-\beta/2\exp[-i(\Omega t-Kx)]. \tag{5}$$

Equation (5) thus describes the three primary diffracted and frequency-shifted orders depicted in Fig. 2. Notice that in Eq. (5) the important SAW amplitude information is contained in the weak ±1 orders. It is, therefore, beneficial to eliminate the large $J_0(\beta)$ term. Notice also that lens L_1 creates a series of spots corresponding to each diffracted beam order, with spot diameters in the frequency filtering plane approximated by

$$D=\frac{2.44\lambda f}{d}, \tag{6}$$

where d is the diameter of the illumination beam, and f is the focal length of the transform lens. In addition, the various diffracted spots are separated by radial distances from the optic axis according to the expression[16]

$$R_{+n}=\frac{n\lambda f}{\Lambda}, \tag{7}$$

where Λ is the SAW wavelength and n is the diffracted order. The use of an appropriate spatial filter mask, with a mask opening determined by Eq. (6), and relative position determined by Eq. (7), will thus filter out unwanted light and allow the diffracted order of interest to pass.

The ability to further discriminate the SAW signal from other unwanted scattered components is provided by the second key feature of the frequency-translated holography measurement process, which involves frequency translating the reference wave. For identical reference and object wave frequencies, the interference fringes produced in the hologram are stationary, enhancing fringe visibility and contrast as the hologram is exposed. Conversely, for reference and object waves with different temporal frequencies, fringes formed in the hologram are traveling wave structures. This causes the film to record reduced fringe visibility due to smearing of the fringes as the hologram is exposed.

For frequency-translated holography, the holographic frequency-filtering process is accomplished by frequency shifting the reference wave to match the shift introduced in the object wave by the SAW. This is traditionally accomplished by placing an AO modulator system in the reference beam path. The AO modulator diffraction process involves the angular separation of frequency-shifted orders, allowing the diffracted order of interest to be passed while the others are blocked. The resulting reference beam provided by an AO modulator system can then be described in phasor form by

$$E_{AO}\propto J_{+1}(\beta_{ref})\exp(i\Omega t), \tag{8}$$

where we assume that the $+1$ diffracted order has been selected, while the phase modulation index β_{ref} is dependent on the characteristics of the AO modulator system parameters.

For holographic recording, the frequency-translated object and reference waves interfere in the recording medium and create a hologram with an exposure distribution governed by the following expression

$$I\propto\langle|E_{ref}+E_{obt}|^2\rangle=\left\langle\left|J_{+1}(\beta_{ref})\exp(i\Omega t)+\frac{\beta}{2}\exp[i(\Omega t-Kx)]\right|^2\right\rangle. \tag{9}$$

This in turn reduces to the well-known four-term holographic exposure expression given by

$$I\propto J_{+1}(\beta_{ref})^2+\frac{\beta^2}{4}+J_{+1}(\beta_{ref})\frac{\beta}{2}\exp(-iKx)+J_{+1}(\beta_{ref})\frac{\beta}{2}\exp(+iKx), \tag{10}$$

where the last two terms are responsible for the real and virtual images, respectively.

Assuming the exposure is linearly recorded as an amplitude transmittance, the holographic reconstruction will produce output waves proportional to the four terms on the right-hand side of Eq. (10). When the reconstruction wave is of the same spatial form as the original reference wave, the last exposure term in Eq. (10) gives the virtual image, which provides a visualization of the SAW.

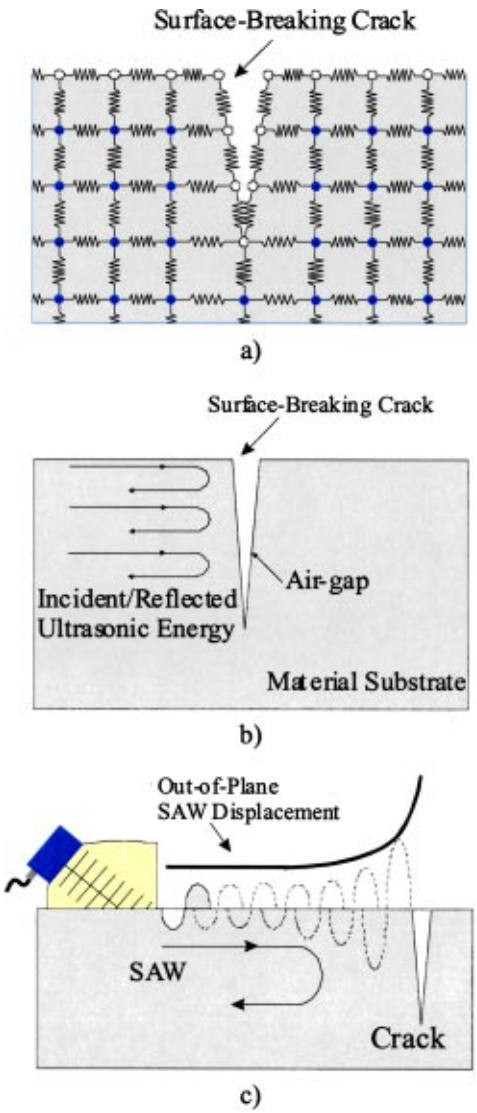

Fig. 3 (a) Spring-mass representation of a surface-breaking crack; (b) ultrasonic reflection from a surface-breaking crack; and (c) schematic diagram showing near-field intensification of ultrasonic displacements near a free-boundary (surface-breaking crack).

2.3 *Crack Imaging Based on Near-Field Ultrasonic Scattering Processes*

Near-field ultrasonic crack scattering effects are based on free-boundary reflection processes that create a local intensification of the ultrasonic displacement field in the immediate vicinity of a surface-breaking crack site.[9] As shown in Fig. 3(a), a surface-breaking crack has two potential free boundaries represented by the opposing crack faces. In a simple spring-mass analysis, the top surface of the material and both crack faces represent tension-free spring systems uncoupled to the areas both above the material surface and within the crack opening.

The free surfaces oscillate differently than the bulk material, and support the propagation of ultrasonic energy by different mechanisms. When an incident ultrasonic pulse arrives at a free boundary, the particles are free to move because of the lack of material (and resistive forces) further upstream. In a spring-mass sense, the particles respond to the tension/compression forces imposed by the incoming wave without restrictions, pulling on the particles they are connected to and stretching the spring-mass bonds. When the incoming ultrasonic pulse reaches the surface-breaking crack, a reflected pulse is created with the same sign and amplitude as the incident pulse [Figs. 3(b) and 3(c)]. The incident and reflected pulses thus reinforce each other, creating an antinode at the free boundary that has a nominal peak displacement that is twice the amplitude of either of the individual pulses [Fig. 3(c)]. The interferometric and holographic NDE systems provide a capability for measuring this local displacement increase, and generate a displacement-field image where the crack site appears as a local brightness increases.

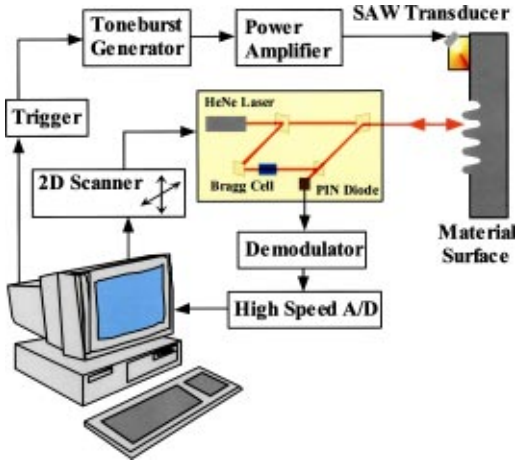

Fig. 4 Schematic diagram of the near-field scanning interferometry (NFSI) system.

3 Experimental Methods

The near-field scanning interferometry (NFSI), and frequency-translated holography (FTH) systems provide a capability for measuring out-of-plane displacements on a material surface with high sensitivity and spatial resolution. The basic interferometry system provides a measurement of the displacement level at a single point as a displacement versus time signal output. A complete 2-D displacement-field image is created by raster scanning the position of the probe beam relative to the sample surface. The holography system, in contrast, provides a complete, full-field image of the displacement field in a single exposure in μs to ms timescales.

The two measurement systems are complementary in nature. The interferometry system, for example, provides much more information in a given measurement (a complete time versus displacement history) than the holography system (a single snapshot of the SAW displacement pattern). The holography system does, however, provide a complete measurement in a very short time, while the interferometry system takes minutes to hours to complete its raster-scan process. The interferometry system also has a significant advantage with respect to signal to noise, when signal isolation, in-line averaging, and time gating is applied to the measured signal.

A schematic diagram of the NFSI system is presented in Fig. 4. The system is built around a commercially available

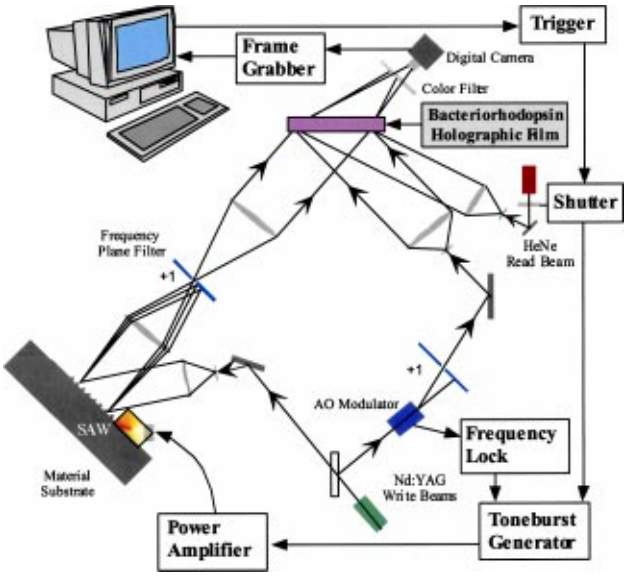

Fig. 5 Schematic diagram of the real-time, frequency-translated holography (FTH) system.

heterodyne interferometry system,[21] which probes the sample surface at a single point. The system uses a 1-mW HeNe laser, and a variable-focus lens to provide spatial resolutions of ~5 μm, and standoff distances from 10 cm to >1 m. Optical heterodyning is provided by a 40-MHz acousto-optic Bragg cell placed in the reference beam path. The resulting instrument is capable of making sensitive displacement measurements in the frequency band 25 kHz to 20 MHz, with subnanometer sensitivities.

A computer-controlled x-y scanning system allows 2-D displacement field images to be obtained. At each scan position, the computer provides a trigger signal to a toneburst generator, which in turn supplies a sinusoidal ac voltage toneburst to drive the SAW transducer. The interferometry system then senses the out-of-plane motion at the focused spot position, and provides a displacement versus time signal to the control software. The detected signal is time gated and phase locked to the original drive signal, providing a measure of the absolute amplitude and phase at each measurement point. The system has a scan precision of 1 μm, and can scan at speeds of three data points per second. A typical measurement of 100×100 points takes approximately 1 h.

A schematic diagram of the frequency-translated holography (FTH) system is provided in Fig. 5. Holograms are written to a real-time holographic film called bacteriorhodopsin (bR)[22–24] using a 100-mW Nd:YAG laser operating at a wavelength of λ=532 nm. The bR film requires an exposure time of between 50 μs to 500 ms, depending on the optical power density incident on the film. A maximum diffraction efficiency of 2.6% was obtained, for example, with an optical power density level of 8.1 mW/cm^2. The bR sample in this instance was a 1-in.-diam, 100-μm-thick film manufactured by Wacker MIB GmbH (model WT1N5; optical density of 5.0 at λ=570 nm).

Frequency shifting of the reference beam is accomplished using a tunable acousto-optic modulator, which is phase locked to the SAW driver. The frequency-plane filter used in the object leg of the holographic recording system consists of an adjustable slit placed in the back focal plane of lens L_1. The slit's width and transverse position then determine which diffracted order is passed to the recording medium through lens L_2. A slit width of 50 μm and transverse position of 200 μm permitted surface acoustic waves in the low MHz range to be studied.

The hologram is read out in real-time using a Bragg-matched, 35-mW HeNe laser operating at 632 nm. A mechanical shutter inserted in the HeNe laser path provides additional control of the read beam. The reconstructed holographic light is finally imaged onto a digital camera system, which uses a simple color filter to block unwanted Nd:YAG (532-nm) light. A frame grabber system then transfers the captured SAW and crack images, in real time, to a computer for display and storage.

4 Results and Discussion

The NFSI and FTH systems each provide a capability for imaging ultrasonic displacement fields on a material surface as 8-bit, gray-level images. In effect, large out-of-plane displacements are mapped to bright regions in the image fields, while small displacement images are dark. For crack detection and characterization purposes, the systems identify cracks according to the localized increase in the displacement field relative to the nominal displacement levels present on the material surface. This manifests itself in the displacement-field images as an observable brightness increase in the immediate vicinity of the crack sites.

4.1 *Crack Imaging Using NFSI and FTH*

Figure 6 provides an example of the crack imaging capabilities of the NFSI measurement system. This figure depicts a digital microscope image [Fig. 6(a)], and a displacement field image [Fig. 6(b)] of a sharp, tight fatigue crack in an aluminum substrate material. The digital and NFSI images correspond to the same 2.7×2.0-mm region on the material surface. Although scratches and surface roughness features can be seen in the digital microscope image, there is no visible evidence of the crack. This is typical of tight fatigue cracks present in aerospace materials, and is one of the reasons they are so problematic. A significant and distinct brightness increase was observed, however, in the NFSI displacement field image [Fig. 6(b)], which allowed the position and microscopic features of the crack site to be observed.

The NFSI image in Fig. 6(b) was generated using a 5-MHz SAW propagating from left to right in the image field. The incident SAW had a nominal peak displacement of 2.73±0.11 nm, while the peak displacement level detected near the crack site was approximately 4.6±0.44 nm. This corresponds to an increase in the out-of-plane displacement level near the crack of 170%, permitting the crack to be easily distinguished from the incident background SAW displacement levels. In fact, the crack formed a distinct boundary, beyond which little or no ultrasonic displacement energy was observed. In this particular instance, the crack was significantly deeper than the penetration depth of the SAW (6-mm-deep crack versus 600-μm SAW penetration depth), causing nearly all of the SAW energy to be reflected. This resulted in a darkened region to

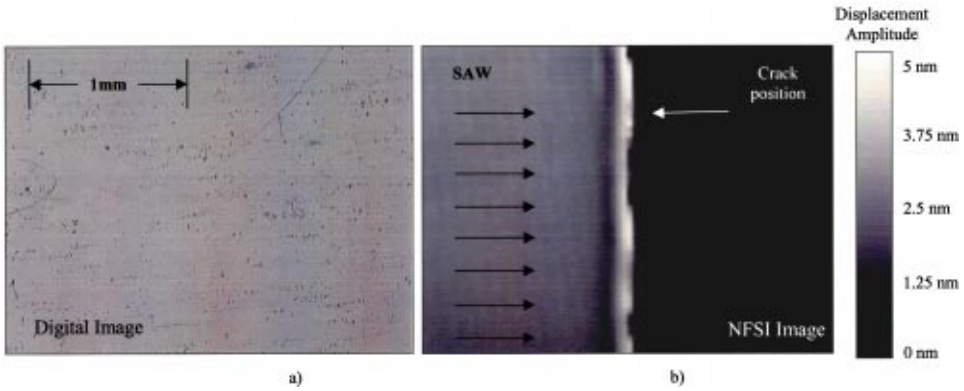

Fig. 6 (a) Digital image; and (b) ultrasonic displacement-field image of surface-breaking crack taken with the NFSI system.

the right of the crack site, where no displacement energy was observed, and an additional increase in the crack image contrast.

Figure 7 provides three additional crack imaging examples taken with the NFSI and FTH systems, respectively. The cracks in this case included: 1. a sharp, through-the-thickness crack in aluminum; 2. a wavy, surface crack in aluminum; and 3. a small, localized fatigue crack in titanium. A 5-MHz SAW was used in each measurement. The SAW had a nominal peak displacement level of 8 to 10 nm, and was incident from the top of each image field, propagating downward.

In all cases, the cracks in Fig. 7 can be easily distinguished from background displacement levels, where a significant increase in the image brightness occurred within ~100 to 200 μm of each crack site. The out-of-plane displacement increase near each of the crack sites was between 120 to 230%. We see that the scanning interferometry and real-time holography systems provide similar crack-imaging capabilities, allowing the detailed structure of each crack to be followed with microscopic precision. We also note that the through-crack and small fatigue crack measurements depicted in Fig. 7 represent tight cracks that were not visible to the naked eye, and were not easily seen even at an optical magnification of 100×. The NFSI and FTH measurement systems, however, were both able to detect and image all three crack types quite easily with good image contrast and signal-to-noise ratio levels.

4.2 *Comparison of NFSI and FTH Systems*

The NFSI and FTH measurement systems are complementary in nature, with each system having its own particular advantages and disadvantages. There are three major differences between the two systems, including: 1. measurement times; 2. the amount and type of information obtained in each measurement; and 3. the inherent noise in each measurement process. Because the NFSI system involves a raster-scanned, point-measurement process, it has a significant disadvantage with regard to making real-time measurements. The scanning interferometry measurements depicted in Fig. 7, for example, were taken at various scan sizes ranging from 60×60 to 180×180 points. At a measurement speed of three points per second, the total mea-

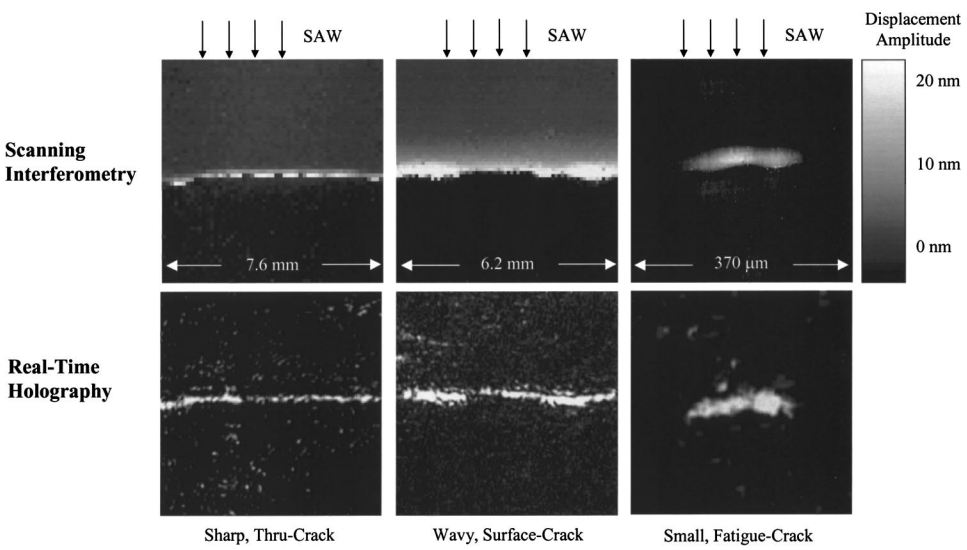

Fig. 7 Comparison of the NFSI and FTH crack-imaging systems for three different types of surface-breaking cracks.

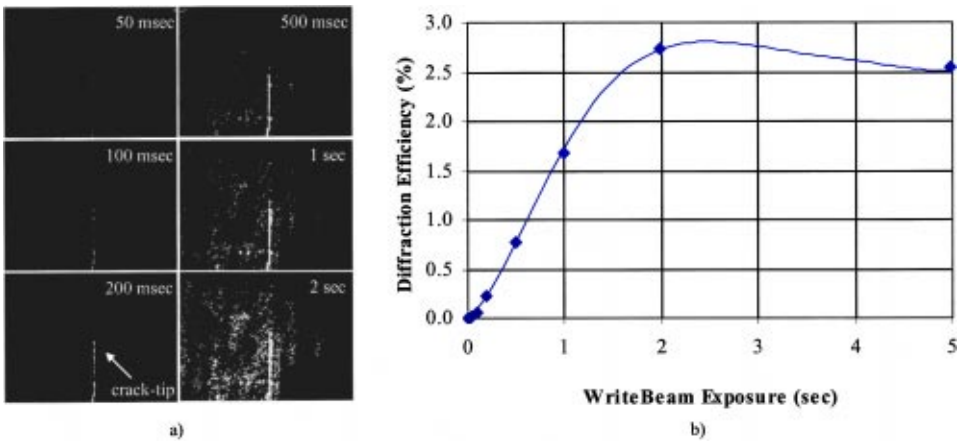

Fig. 8 (a) FTH crack images for increasing exposure times; and (b) bacteriorhodopsin film exposure curve (diffraction efficiency versus exposure time).

surement times ranged from 20 min to 3 h. The same real-time holography measurements required an exposure time of only 250 msec to record. The holography system's time advantage comes at the cost of a significant increase in system complexity, however, as depicted in Fig. 5.

The second important difference between the two systems involves the amount and type of displacement information that is provided in each measurement. The holography system, for example, provides only a *relative* measure of the local surface displacement. This is primarily due to the fact that it time integrates its signal as a function of the holographic film's exposure. For a given surface displacement level, the recorded image brightness will vary with the film exposure time, power density, and bR film type. An example of this is depicted in Fig. 8(a), where a crack tip has been imaged at six different exposure times ranging from 50 msec to 2 sec using a bR film with an optical density of 5.0 at 570 nm (Wacker MIB GmbH WT1N5). The displacement field image intensity and crack-tip image brightness levels are seen to increase with increasing film exposure levels, even though the ultrasonic displacement levels depicted in each image do not change. As shown in Fig. 8(b), the diffraction efficiency of the bR film increases with increasing film exposure times in a linear fashion until approximately 2 sec of exposure. Beyond that, the film begins to saturate due to bleaching effects.[25] Variations in exposure time, power density, and film type will, therefore, impact the diffraction efficiency of the FTH measurement, which in turn results in a relative change in the displacement field image brightness levels.

In contrast to the real-time holography system, the scanning interferometry system provides a complete time-versus-displacement history of an ultrasonic wave as it propagates along the material surface. An example of this is provided in Fig. 9(a), where the specific waveform shape, phase, and *absolute* amplitude levels of a SAW interacting with a crack have been studied in detail. The incident SAW in this particular case was a 5-MHz impulse that had approximately 1.5 cycles, and a nominal peak displacement amplitude of 2.7 nm. The five plots provided in Fig. 9(a) correspond to time-versus-displacement measurements taken at different spatial positions away from the crack site [the specific measurement positions are superimposed on the displacement-field image provided in Fig. 9(b). The information provided in each plot allows the incident SAW, its primary reflection from the crack face, and other auxiliary scattered waves to be studied in detail. In addition, the peak displacement-field image shown in Fig. 9(b) provides

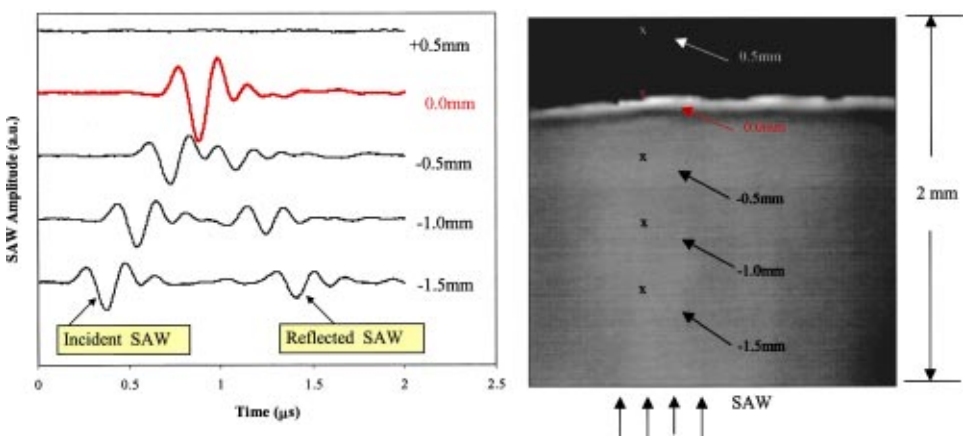

Fig. 9 (a) NFSI time-versus-displacement measurement plots taken at increasing positions away from the crack location; and (b) displacement-field image of the crack.

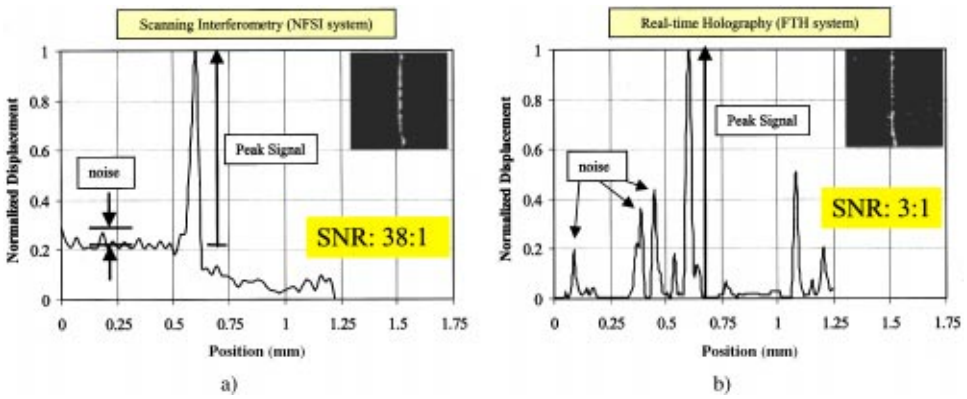

Fig. 10 Crack images depicting system noise effects for (a) the NFSI and (b) FTH systems.

a compact and simple measurement of the crack and its surroundings.

The third major difference between the NFSI and FTH systems involves the inherent noise in each measurement process. As seen in Fig. 7, the real-time holography crack measurements are inherently much noisier than the scanning interferometry measurements. This is unfortunately a problem with most holographic recording systems, and is well documented in the literature.[13–15] The noise in a holographic image can be introduced by many different sources, ranging from environmental sources (vibration and temperature fluctuations), to recording film irregularities (nonuniformity and defects), to extraneous light scattering from dust and optical components. The scanning interferometry system in contrast is somewhat immune to all of these considerations, because it is limited primarily to a single-point, light-scattering event, and takes place in the electronic time domain. Once the interferometric signal has been detected and converted from an optical intensity to an electronic signal, sophisticated signal processing techniques can also be applied to greatly enhance the signal-to-noise ratio (SNR) for an individual measurement point. In-line averaging, frequency-based filtering, and time-gated detection are three of the techniques that were applied in the NFSI system to improve SNR levels.

Figure 10 provides a direct comparison of the NFSI and FTH crack imaging systems, where an estimate of noise and SNR has been provided for each image case. The line plots correspond to a cross-sectional cut taken through the center of each image, normal to the crack orientation for the NFSI [Fig. 10(a)], and FTH [Fig. 10(b)] systems. The displacement peaks at the axial positions of ~0.6 mm (see the interferometric and holographic inset figures and plots in Fig. 10) are due to the near-field ultrasonic crack scattering effect, which resulted in SNR ratio levels of ~38:1 for the interferometric measurement, and ~3:1 for the holographic measurement. The auxiliary peaks in the holographic measurement [Fig. 10(b)] occurred at random positions throughout the image field. Notice, however, that although the holographic image appears noisier than the interferometric image, the crack in the holographic image is sharper in contrast to the background levels, and may be considered as more visually appealing to some, a subjective effect that is not without merit. Image processing could also be used in both image cases to further isolate and enhance the crack images.

In addition to measurement time, type, and SNR, there are several additional considerations for each measurement system that can impact their ability to image microscopic cracks. These are highlighted in Table 1. Spatial resolution in particular is a primary consideration for both systems, and is fundamentally limited to an optical diffraction limit of approximately one micron. The resolution of the scanning interferometry system is essentially limited by the focused spot size of the probe beam (approximately 5 μm), while the FTH system is limited by the characteristics of

Table 1 Comparison of NFSI and FTH crack-imaging measurement systems.

Parameter	Scanning interferometry	Frequency-translated holography
Displacement type	Absolute displacement amplitude	Relative displacement amplitude
Displacement sensitivity	Sub-angstrom	Nanometer
Displacement range	$<10^{-10}$ to 10^{-7} m	10^{-9} to $>10^{-6}$ m
Signal to noise	~38:1	~3:1
Measurement type	Complete time history at each point	Time-integrated (50 μs to 500 ms)
Measurement time	3 points per second (minutes–hours)	50 μs–500 ms (fluence dependent)
Spatial resolution	Focused spot size of ~5 μm	Imaging resolution of ~14 μm
System complexity	Relatively simple	Relatively complex
Imaging capability	Single point, raster scanned	Full-field image
Time-resolved measure	Time-resolved (microsecond)	Time-integrated only

the imaging system used. For the holographic images presented in Figs. 7, 8, and 10, a 4-f lens system was used that utilized a pair of 2-in.-diam, 200-mm focal length lenses, providing a 1:1 magnification factor and an estimated resolution of ~14 μm. The scanning interferometry system also has a 1 to 2 order of magnitude advantage in displacement sensitivity, which would potentially allow it to detect very small, microscopic cracks.

5 Conclusions

The combination of advanced interferometric and holographic displacement measurements with classical ultrasonic testing methods provides powerful new NDE methods for microcrack detection and characterization. In this effort, advanced scanning interferometric and real-time holographic NDE systems are developed and used to detect and characterize microcracks through near-field ultrasonic scattering and free-boundary reflection processes. Surface-breaking cracks produce local increases in the ultrasonic displacement levels that are imaged using the interferometric and holographic NDE systems. The interferometric and holographic imaging approaches provide noncontact and optical-diffraction-limited measurement capabilities that are essential for probing ultrasonic displacement fields in the immediate vicinity of cracks. Several representative crack-imaging results have been provided, along with detailed descriptions of both experimental techniques, as well as a comparison of the capabilities and limitations of each method. Both advanced NDE systems provide very powerful means for evaluating surface-breaking cracks in detail.

Acknowledgments

The authors gratefully acknowledge the Center for Materials Diagnostics (CMD) at the University of Dayton for financial and facility support, and the DARPA NDE-MURI program (under AFOSR Grant number F49620-96-1-0442) for financial support. The authors would also like to thank Dr. Shamachary Sathish for his important contributions to the basic understanding of near-field ultrasonic crack-scattering processes.

References

1. L. Cartz, *Nondestructive Testing*, ASM International, Materials Park, OH (1996).
2. B. Hull and V. John, *Non-Destructive Testing*, Springer-Verlag, New York (1988).
3. J. Kim and S. Rokhlin, "Surface acoustic wave measurements of small fatigue crack initiated from a pit," *Int. J. Solids Struct.* **39**, 1487–1505 (2001).
4. D. Hagemaier and G. Kark, "Eddy current detection of short cracks under installed fasteners," *Mat. Eval.* **55**, 25–30 (Jan. 1997).
5. J. Polak, K. Obrtlik, and A. Vasek, "Short crack growth kinetics and fatigue life of materials," *Mater. Sci. Eng., A* **234–236**, 970–973 (1997).
6. R. Thompson and D. Thompson, "Ultrasonics in nondestructive evaluation," *Proc. IEEE* **73**, 1716 (1985).
7. M. Resch, "Use of nondestructive evaluation techniques in studies of small fatigue cracks," *Basic Questions in Fatigue*, **1**, **ASTM STP 924**, 323–336 (1988).
8. M. Blodgett, W. Hassan, and P. Nagy, "Theoretical and experimental investigation of the lateral resolution of eddy current imaging," *Mater. Eval.* **58**, 647–654 (2000).
9. J. Blackshire and S. Sathish, "Near-field ultrasonic scattering from surface-breaking cracks," *Appl. Phys. Lett.* **80**(18), 3442–3444 (2002).
10. J. Blackshire, S. Sathish, B. Duncan, and M. Millard, "Real-time, frequency-translated holographic visualization of surface acoustic wave interactions with surface-breaking defects," *Opt. Lett.* **27**(12), 1025–1027 (2002).
11. J. Moulder, N. Nakagawa, K. No, Y. Lee, and J. McClelland, "Photoinductive imaging: a new NDE technique," in *Review of Progress in Quantitative NDE*, 8A, D. Thompson and D. Chimenti, Eds., Plenum, New York (1989).
12. L. Favro, R. Thomas, X. Han, Z. Ouyang, G. Newaz, and D. Gentile, "Sonic infrared imaging of fatigue cracks," *Int. J. Fatigue* **23**, 471–476 (2001).
13. C. Scruby and L. Drain, *Laser Ultrasonics—Techniques and Applications*, Adam Hilger Publishing Ltd., Bristol, England (1990).
14. R. Erf, *Holographic Nondestructive Testing*, Academic Press, New York (1974).
15. *Nondestructive Testing Handbook, Vol. 9, Special Nondestructive Testing Methods*, P. Morre and P. McIntire, Eds., ASNT Press, New York (1995).
16. B. Duncan, "Visualization of surface acoustic waves by means of synchronous amplitude-modulated illumination," *Appl. Opt.* **39**(7), 2888–2895 (2000).
17. C. Aleksoff, "Temporally modulated holography," *Appl. Opt.* **10**(6), 1329–1341 (1971).
18. T. Nakajima, "Detection of small amplitude vibrations by modulated reference wave holography," *Jpn. J. Appl. Phys.* **13**(3), 471–483 (1974).
19. S. Shiokawa, T. Moriizumi, and T. Yasuda, "Study of SAW propagation characteristics by frequency-translated holography," *Appl. Phys. Lett.* **27**(8), 419–420 (1975).
20. M. Abramowitz and I. Stegun, *Handbook of Mathematical Functions*, Dover Publications, New York (1972).
21. *Polytec OFV-302 Operator's Manual*, Polytec GmbH, Waldbronn, Germany (1997).
22. D. Oesterhelt, C. Brauchle, and N. Hampp, "Bacteriorhodopsin: a biological material for information processing (March 1974)," *Q. Rev. Biophys.* **24**(4), 425–478 (1991).
23. N. Hampp, A. Seitz, T. Juchem, and O. Dieter, "Large-diameter bacteriorhodopsin films for applications in non-destructive testing," *Proc. SPIE* **3623**, 243–251 (1999).
24. C. Fitzpatrick, "The erasable material bacteria rhodopsin: Its characteristics and uses in holographic applications," *Proc. SPIE* **1667**, 225–232 (1992).
25. Z. Dancshazy, Z. Tokaji, and A. Der, "Bleaching of bacteriorhodopsin by continuous light," *FEBS Lett.* **450**, 154–157 (1999).

James L. Blackshire received his MS and PhD degrees in electro-optics from the University of Dayton in 1991 and 2003, respectively. He currently works as a research scientist for the Air Force Research Laboratory in the area of nondestructive evaluation (NDE) of aerospace materials. His main research interests involve the development and integration of novel NDE systems for the detection and characterization of microcracks, material fatigue, and corrosion in structural aerospace components.

Bradley D. Duncan received the PhD degree in electrical engineering from Virginia Polytechnic Institute and State University (Virginia Tech) in 1991, after which he joined the University of Dayton (UD) faculty. He is now a tenured (full) professor of electrical and computer engineering, with a joint appointment in the graduate electro-optics program. His research interests and activities span a wide range of areas within the optical sciences, including the study of ladar systems, photorefractive applications, fiber optic sensor and system technology, integrated optics, nondestructive evaluation,and scanning and nonlinear optical image processing. He is a mem-ber of the OSA, SPIE, and ASEE. He is also a senior member of IEEE. He has previously served as the book reviews editor for *Optical Engineering* (the international journal of SPIE), and is the faculty advisor for both the University of Dayton student chapter of the OSA, and EΔT—UD's engineering social fraternity. He directs the research conducted in the UD's NSF Photonics Laboratory, and in 1998 won the "Engineering Best Professor of the Year" award.